Electronic Supplementary Information for

Photoelectrochemical water-splitting using GaN pyramidal dots and its long-term stable characteristics in two-electrode configuration

Sangmoon Han,† Siyun Noh, Jaehyeok Shin, Yeon-Tae Yu, In-Seok Seo, and Jin Soo Kim*

Department of Electronic and Information Materials Engineering, Division of Advanced Materials Engineering, and Research Center of Advanced Materials Development, Jeonbuk National University, Jeonju 54896, South Korea.

†Present address: Mechanical Engineering & Materials Science, Washington University in Saint Louis, MO, 63130, USA.

*Corresponding author: (e-mail) kjinsoo@jbnu.ac.kr; (Tel.) +82-63-270-2291; (Fax) +82-63-270-2305

Characterization of GaN pyramidal dots (PDs) coated with oxidized tungsten sulfide (OTS)

For the formation of the OTS layer from tungsten sulfide (W_xS_{1-x}) covering GaN PDs, the annealing treatment was conducted using a rapid thermal annealing (RTA) system with a model of Nextron. A field-emission scanning electron microscopy (FE-SEM), an x-ray diffraction (XRD), a high-resolution transmission-electron microscopy (HR-TEM), and x-ray photoelectron spectroscopy (XPS) were used to analyze the structural properties of the GaN PDs and photoanode samples. The FE-SEM with a model of Hitachi Su-70 was used and its accelerating voltage was set to 10 kV. The XRD rocking curves of the samples were obtained using a model of MAX-2500 with a wavelength of Cu K_α. The HR-TEM system with a model of Jeol Jem-arm 200F was used to investigate the crystallinity of the samples. The XPS measurements were performed using a model of Thermo Scientific K-Alpha+ XPS spectrometer with a microfocused monochromatic Al K_α source.

For the analysis on the optical properties of the samples, photoluminescence (PL) spectroscopy and an ultraviolet-visible spectrophotometer were used. For PL measurements, a diode-pumped solid-state laser with a wavelength of 266 nm was used as an excitation source. A charge-coupled device was used to detect luminescence from the GaN PDs. A monochromator with a length of 0.5 m was used. An ultraviolet-visible spectrophotometer (UV-2550, Shimadzu) at near-normal incidence (θ = 8°) was used to obtain the absorption spectrum, where the slit size was set to 5 nm.

The photoelectrochemical water splitting (PEC-WS) was conducted in a three-electrode cell. The Pt mesh structure (2.5×2.5 cm^2) and Ag/AgCl were used as a counter electrode and a reference electrode, respectively. The 0.5-M H_2SO_4 was used as the electrolyte. A xenon lamp (MAX-303) was used as a light source, where the light intensity was fixed to 100 mW/cm^2. The active area of the photoanodes was 0.5×0.5 cm^2. The PEC-WS performances were recorded using a Reference 3000 potentiostat (Gamry Instruments) at the potential bias of (-)1.25 to 1.23 V.

Summary on the PEC-WS performances of previous photoanodes

Photoanode	Current density [mA cm^{-2}]	Electrolyte	STH [%]	Retention rate	Reference
Porous GaN	0.41 (0.6 V vs Ag/AgCl)	1 M-NaOH	-	80.4% in 1 h	S1
ZnS/GaN	~ 6 (0.5 V vs RHE)	1 M-NaOH	-	91% in 6 h	S2
GaN with Co-Pi	1.1 (1.2 V vs RHE)	0.1 M-KPi	-	54.5% in 1 h	S3
InN/InGaN	12.7 (0 V vs RHE)	0.5 M-Na_2SO_4	-	~98% in 1 h	S4
CoPi/GaN/Ta_3N_5	8 (1.2 V vs RHE)	0.5 M-KPi	1.5 at immediately after the fabrication	79.1% in 10 h	S5
InGaN nanorods with C_3N_4	2 (0.6 V vs RHE)	0.5 M-H_2SO_4	-	67% in 2 h	S6
CdSe/ZnO nanowire array	14.9 (0.8 V vs RHE)	50-mM $NaOH_3$	-	86.2% in 1 h	S7
WO_3/Bi_2S_3	1.3 (1.2 V vs Ag/AgCl)	0.5-M Na_2S	-	69% in 1 h	S8
Bi_2S_3/RGO-TiO_2	2.7 (1.23 V vs RHE)	0.25-M Na_2S	-	66% in 1h	S9
CdS/ZnS	7.8 (0 V vs RHE)	0.25-M Na_2S	-	89.23% in 15 min	S10
$SrTaO_2N$/CoPi	1.2 (1.23 V vs RHE)	1-M NaOH	-	75% in 1 h	S11
$BaTaO_2N$/Co	4.2 (1.23 V vs RHE)	0.2-M KH_2PO_4	-	80% in 6 h	S12
$BiVO_4$-Sb_2Se_3	1.2 (0 V vs Pt)	0.5-M K_2HPO_4 + 0.01-M V_2O_5	~ 1 for 10 h	75% in 10 h	S13
$CdIn_2S_4/In_2S_3/SnO_2$	2.68 (0 V vs Pt)	0.25-M Na_2SO_3 /0.25-M Na_2S3	2.3 for 1.6 h	69% in 1.6 h	S14
Perovskite-$BiVO_4$/CoPi	3.0 (0 V vs MoS_x)	0.5-M $Co(NO_3)_2$	2.3 for 6 h	66% in 10 h	S15
BiVO4/FeOOH /NiOOH	3.2 (0.6 V vs RHE)	V^{5+}-saturated electrolyte	-	~96% in 500 h	S16
$BiVO_4$	~ 1 (0 V vs Cu_2ZnSnS_4)	0.25-M Na_2SO_3 /0.25-M Na_2S (Hole scavengers)	1 for 10 h	-	S17

Table 1. Summary on the PEC-WS performances of the previous photoanodes.

FE-SEM images of the photoanodes

Fig. S1a-d show the three-dimensional (left) and expanded (right) FE-TEM images of the GaN-PD/W_xS_{1-x} and GaN-PD/OTS photoanodes fabricated with three different RTA times of 30 (GaN-PD/OTS-30), 60 (GaN-PD/OTS-60), and 90 min (GaN-PD/OTS-90), respectively. The morphologies of the GaN-PD/W_xS_{1-x} and GaN-PD/OTS nanostructures were well retained after forming the W_xS_{1-x} and OTS layer, compared to those of the pristine GaN PDs.

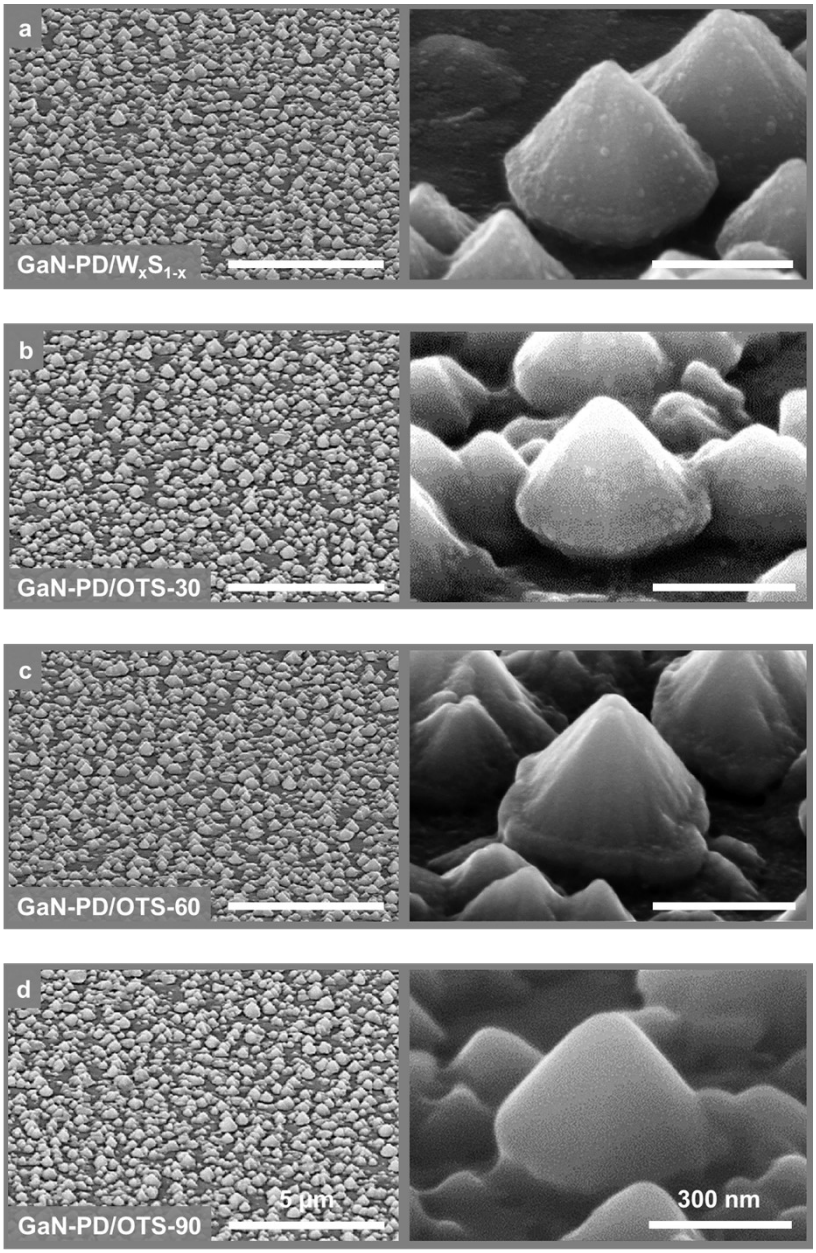

Fig. S1. Three-dimensional (left) and expanded (right) FE-SEM images of the (a) GaN-PD/W_xS_{1-x}, (b) GaN-PD/OTS-30, (c) GaN-PD/OTS-60, and (d) GaN-PD/OTS-90.

HR-TEM images of the photoanodes

Fig. S2a-d show the HR-TEM images of the GaN-PD/W_xS_{1-x}, GaN-PD/OTS-30, GaN-PD/OTS-60, and GaN-PD/OTS-90 photoanodes, respectively. The average thickness of the W_xS_{1-x} layer was measured to be 5.14 nm for the GaN-PD/W_xS_{1-x} photoanode shown in Fig. S2a. The average thicknesses of the OTS layer for the GaN-PD/OTS-30, GaN-PD/OTS-60, and GaN-PD/OTS-90 were measured to be 5.22, 5.23, and 5.25 nm, respectively. The thicknesses of the OTS layer slightly increased with increasing RTA time because of the rearrangement and the compensation of sulfur vacancies in the O_2 atmosphere.[S18]

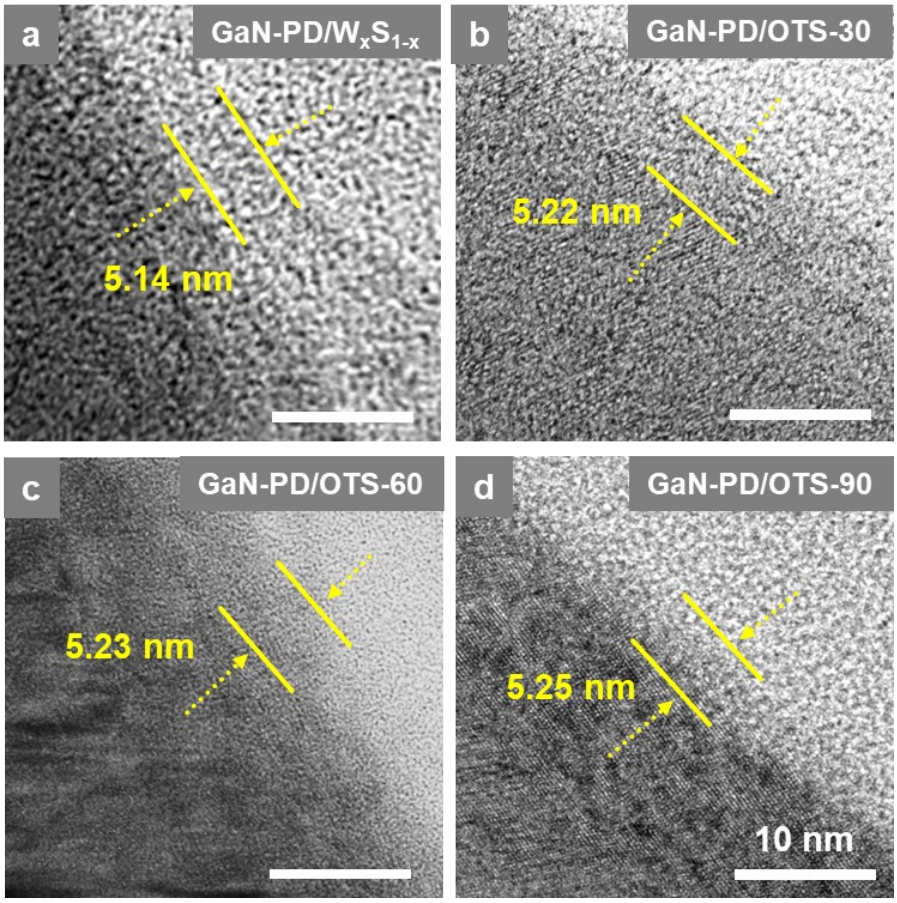

Fig. S2. HR-TEM images of the (a) GaN-PD/W_xS_{1-x}, (b) GaN-PD/OTS-30, (c) GaN-PD/OTS-60, and (d) GaN-PD/OTS-90.

PEC-WS performances of the photoanodes

Fig. S3a and b show the current density (*J*)-voltage (*V*) characteristic curves of the GaN-PD, GaN-PD/W_xS_{1-x}, GaN-PD/OTS-30, GaN-PD/OTS-60, and GaN-PD/OTS-90 photoanodes under dark and illumination conditions. Under dark, the current densities of GaN-PD, GaN-PD/W_xS_{1-x}, GaN-PD/OTS-30, GaN-PD/OTS-60, and GaN-PD/OTS-90 photoanodes were measured to be 0.1, 28.9, 21.1, 19.5, and 9.7 μA/cm^2, respectively, at the potential of 0.6 V vs. reversible hydrogen electrode (RHE). Under illumination, the current densities of the GaN-PD, GaN-PD/W_xS_{1-x}, GaN-PD/OTS-30, GaN-PD/OTS-60, and GaN-PD/OTS-90 photoanodes were measured to be 0.1, 1.8, 1.5, 1.2, and 1.1 mA/cm^2, respectively, at 0.6 V vs. RHE. Fig. S3c shows the applied bias photon-to-current efficiency (ABPE) of the photoanodes calculated from the *J-V* characteristic curves. The maximum ABPEs of the GaN-PD, GaN-PD/W_xS_{1-x}, GaN-PD/OTS-30, GaN-PD/OTS-60, and GaN-PD/OTS-90 photoanodes were calculated to be 0.1, 1.2, 1.0, 0.8, and 0.7%, respectively. The stability test of the photoanodes was conducted using a chronoamperometry at 0.6 V vs. RHE, which are shown in Fig. S3d. After three hours of PEC-WS, the current densities of the GaN-PD, GaN-PD/W_xS_{1-x}, GaN-PD/OTS-30, GaN-PD/OTS-60, and GaN-PD/OTS-90 were measured to be 0.1, 0.5, 1.13, 1.18, 1.07 mA/cm^2, respectively, which are equivalent to 99.8, 26.3, 70.6, 98.3, and 98.2% of those obtained immediately after the reaction. The GaN-PD/OTS-60 shows not only high current density and ABPE but also high stability compared to those of other photoanodes.

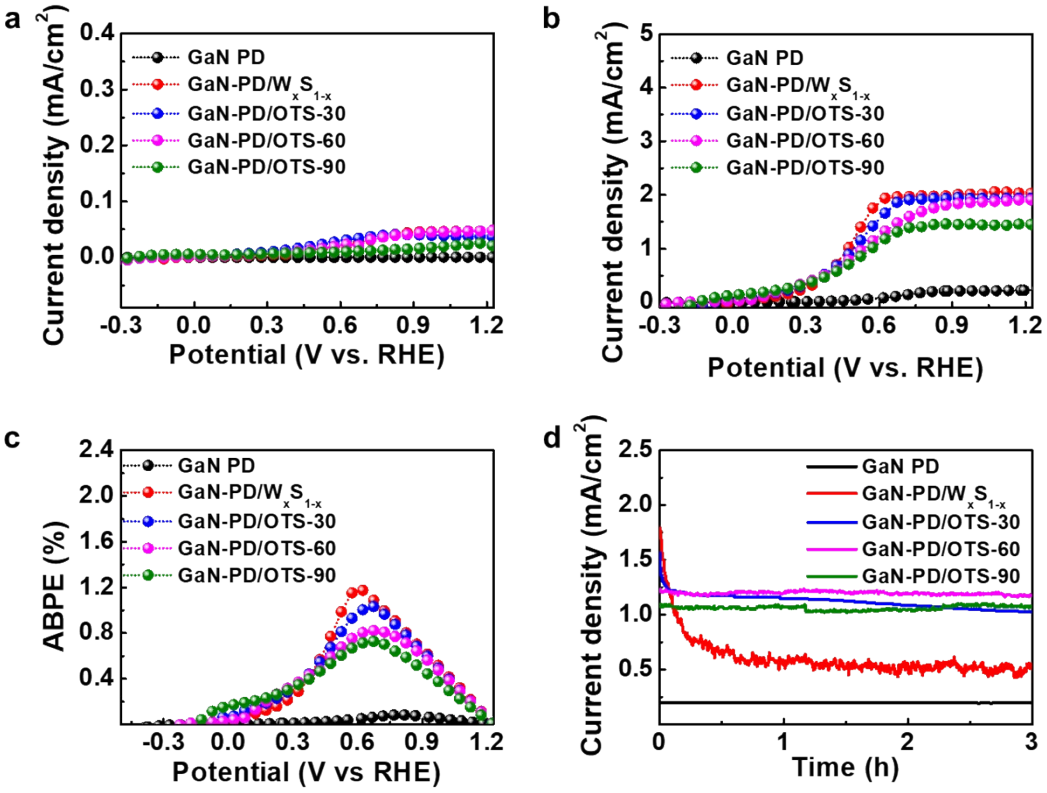

Fig. S3. *J-V* characteristic curves under (a) dark and (b) illumination condition, and (c) ABPEs of the photoanodes. (d) Current density of the photoanodes performed for three hours

FE-SEM images of the photoanodes measured before the reaction and after three hours of the PEC-WS

Fig. S4a-d show the three-dimensional FE-SEM images measured before the reaction and after three hours of PEC-WS of the GaN-PD/W_xS_{1-x}, GaN-PD/OTS-30, GaN-PD/OTS-60, and GaN-PD/OTS-90 photoanodes, where the insets are the expanded images. Before the reaction, the spatial densities of the GaN-PD/W_xS_{1-x}, GaN-PD/OTS-30, GaN-PD/OTS-60, and GaN-PD/OTS-90 nanostructures were calculated to be 7.6±1.7x10^8, 7.8±1.2x10^8, 7.7±0.7x10^8, and 7.7±0.9x10^8 cm^{-2}, respectively. After three hours of PEC-WS, the spatial densities of the GaN-PD/W_xS_{1-x}, GaN-PD/OTS-30, GaN-PD/OTS-60, and GaN-PD/OTS-90 nanostructures were calculated to be 7.5±1.8x10^8, 7.6±0.8x10^8, 7.7±0.7x10^8, and 7.7±1.3x10^8 cm^{-2}, respectively. The shape of the GaN-PD/W_xS_{1-x} and GaN-PD/OTS nanostructures measured after the PEC-WS continued for three hours is similar to their initial one.

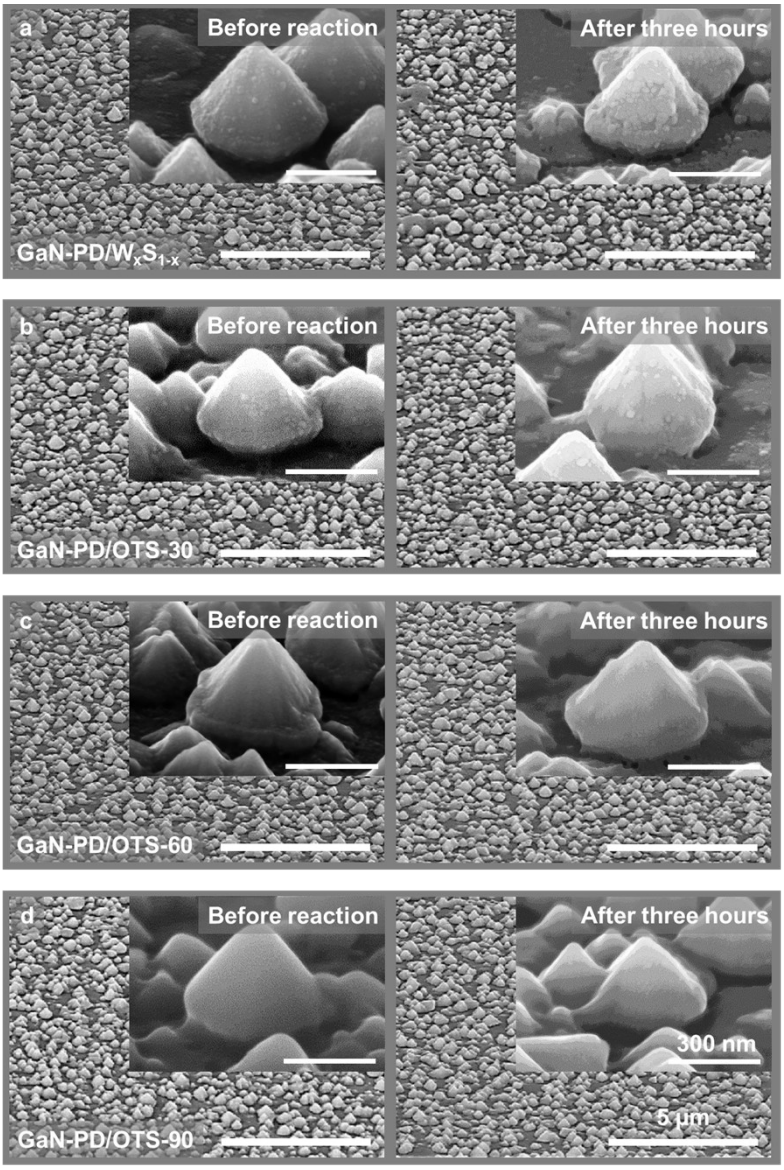

Fig. S4. Three-dimensional FE-SEM images of the (a) GaN-PD/W_xS_{1-x}, (b) GaN-PD/OTS-30, (c) GaN-PD/OTS-60, and (d) GaN-PD/OTS-90 photoanodes measured before the reaction and after three hours of the PEC-WS.

Original XPS curves of the photoanodes before the reaction and after three hours of the PEC-WS

Fig. S5a and b shows the original XPS curves of the photoanodes measured before the reaction and after three hours of the PEC-WS.

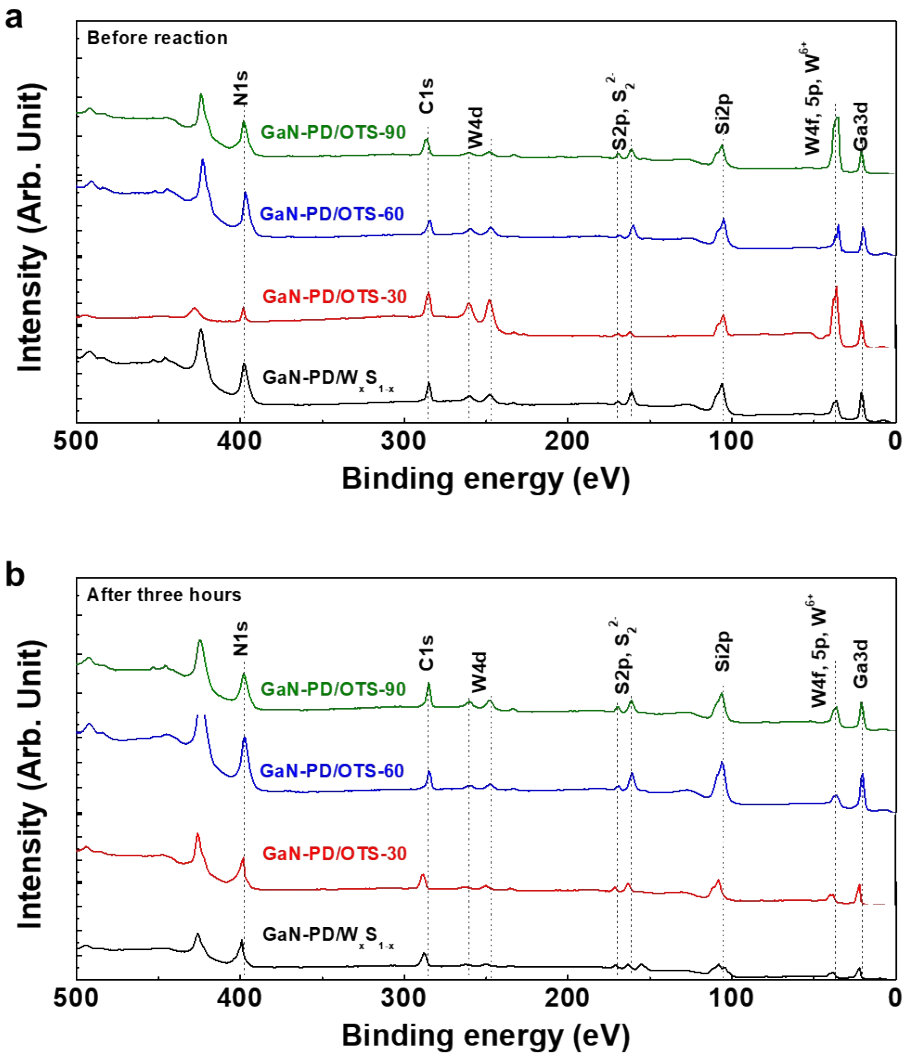

Fig. S5. Original XPS curves of the GaN-PD/OTS photoanodes (a) before the reaction and (b) after three hours of the PEC-WS.

Expanded XPS curves of the photoanodes before the reaction and after three hours of the PEC-WS

Fig. S6 shows the expanded XPS curves of tungsten (W), sulfur (S), oxygen (O), gallium (Ga), and nitrogen (N) for the GaN-PD/W_xS_{1-x}, GaN-PD/OTS-30, GaN-PD/OTS-60, and GaN-PD/OTS-90 photoanodes measured before the reaction and after three hours of the PEC-WS. In Fig. S6a, three W4f peaks after three hours of the PEC-WS were observed at 34.86 (1T-W4f), 36.77 (2H-W4f), and 39.48 eV (W5p3/2), in which the binding energy increase compared to those measured before the reaction. For the 1T-S2p, 2H-S2p, and O vacancy peaks, their binding energy also increases after three hours of the PEC-WS. This result is attributed to the corrosion of W_xS_{1-x}, in which S atoms can react with redox species in the electrolyte.[S19] With increasing the annealing temperature for the GaN-PD/OTS photoanodes, the peak positions of 2H-W4f, W5p3/2, 1T-S2p, and 2H-S2p measured after three hours of the PEC-WS were well consistent with those before the reaction. This result indicates that the W_yO_{1-y} layer formed from the RTA process protects the corrosion of W_xS_{1-x}. After three hours, the binding energies of Ga3d and N1s were measured to be 20.8, and 398.1 eV, which are consistent with those measured before the reaction. With increasing the RTA time, most of the W and S peaks well coincide with those before the PEC-WS reaction.

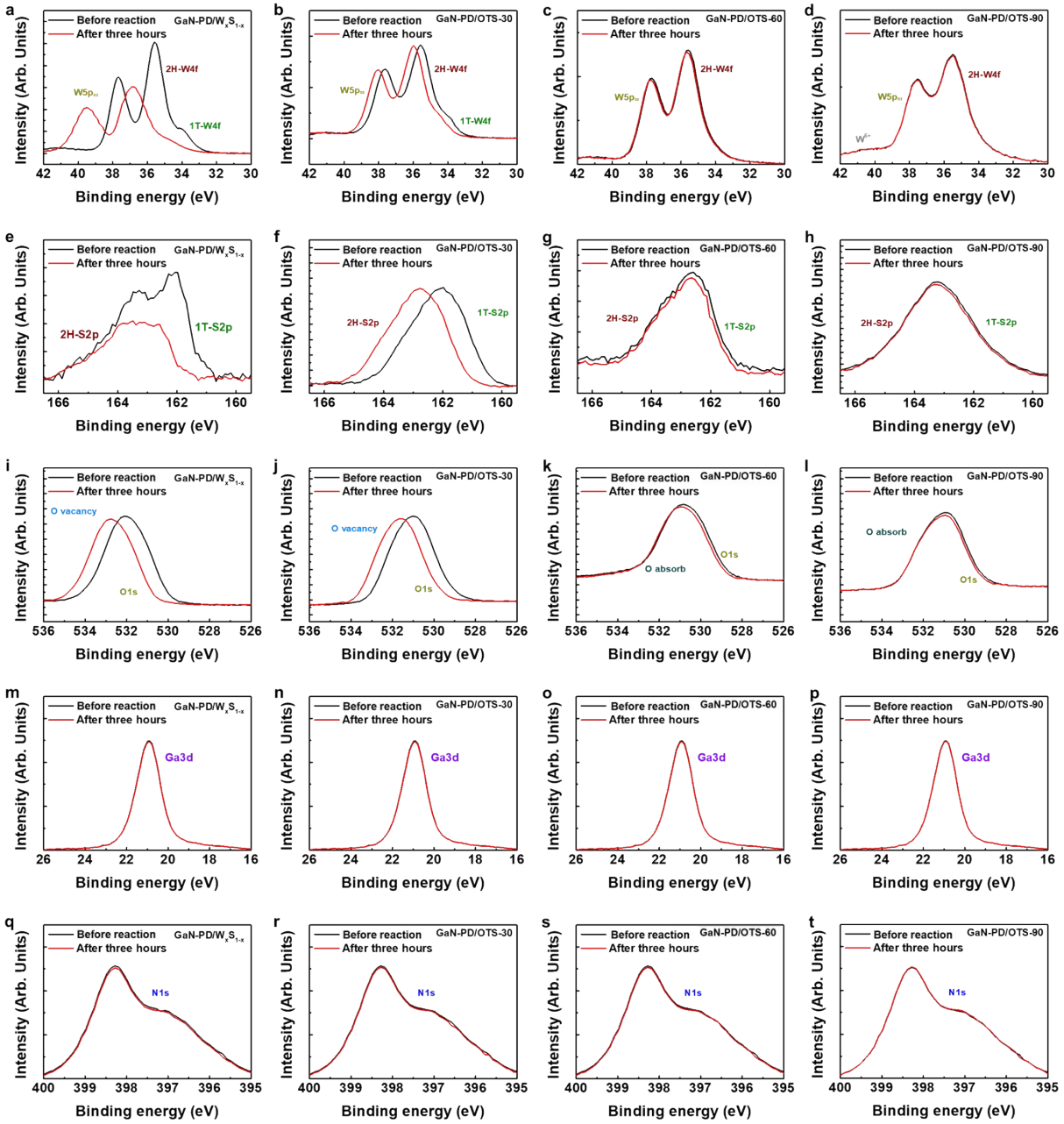

Fig. S6. High-resolution XPS spectra of (a-d) W4f, (e-h) S2p, (i-l) O1s, (m-p) Ga3d, and (q-t) N1s before the reaction and after three hours of the PEC-WS.

Original XPS curve of the GaN-PD/OTS photoanode seven days after the start of the PEC-WS

Fig. S7 shows the original XPS curves of the GaN-PD/OTS photoanode measured after seven days of the PEC-WS.

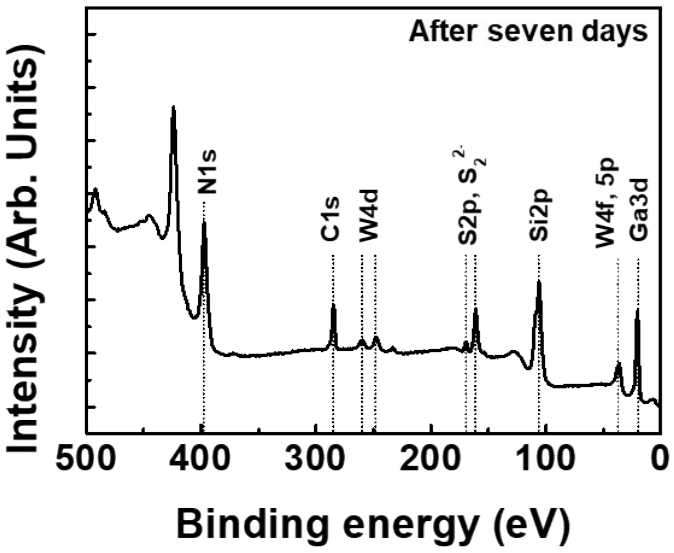

Fig. S7. Original XPS curves of the GaN-PD/OTS photoanode measured after seven days of the PEC-WS.

***J-V* characteristic curve and ABPE of the GaN-PD/OTS photoanode in the two-electrode configuration**

Fig. S8a shows the operating current density of the overall PEC-WS system, estimated by overlapping the *J-V* curves of the GaN-PD/OTS photoanode and the Pt counter electrode measured immediately after the reaction started. Our PEC-WS system shows that the working potential appears to be 0 V vs Pt, where the current density is 1.3 mA/cm^2. This result indicates that the PEC-WS system with the GaN-PD/OTS photoanode is feasible without applying bias.[S20] Fig. S8b and c show the *J-V* characteristic curves and ABPEs of the GaN-PD/OTS photoanode in two-electrode configuration. The current density under dark was measured to be 0.01 mA/cm^2 at 0 V vs. a Pt electrode. Under illumination, the current densities were measured to be 1.30 and 1.26 mA/cm^2 immediately after the reaction and after 20 hours of the PEC-WS at 0 V vs. a Pt electrode, respectively. The maximum ABPEs of the photoanode immediately after the reaction and after 20 hours of the PEC-WS were calculated to be 1.6 and 1.5%, respectively.

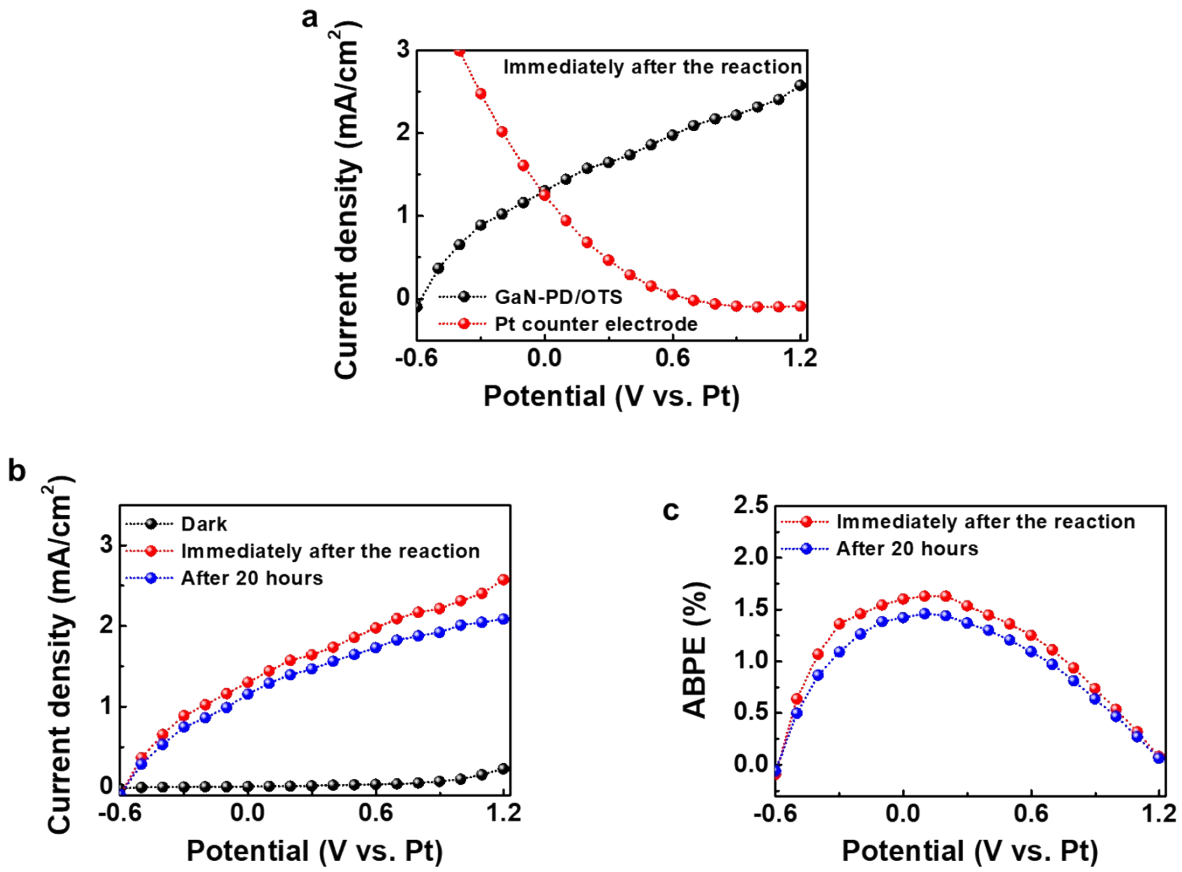

Fig. S8. (a) *J-V* characteristic curves of the GaN-PD/OTS photoanode and the Pt counter electrode. (b) *J-V* characteristic curves and (c) ABPEs of the GaN-PD/OTS photoanode measured in the two-electrode configuration..

References

1. C. Yang, X. Xi, Z. Yu, H. Cao, J. Li, S. Lin, Z. Ma and L. Zhao, Light modulation and water splitting enhancement using a composite porous GaN structure. *ACS Appl. Mater. Interfaces* 2018, **10**, 5492-5497.
2. M. A. Hassan, J.-H. Kang, M. A. Johar, J.-S. Ha and S.-W. Ryu, High-performance ZnS/GaN heterostructure photoanode for photoelectrochemical water splitting applications. *Acta Mater.* 2018, **146**, 171-175.
3. J. Kamimura, P. Bogdanoff, F. F. Abdi, J. Lähnemann, R. van de Krol, H. Riechert and L. Geelhaar, Photoelectrochemical properties of GaN photoanodes with cobalt phosphate catalyst for solar water splitting in neutral electrolyte. *J. Phys. Chem. C* 2017, **121**, 12540-12545.
4. N. U. Alvi, P. E. D. S. Rodriguez, P. Aseev, V. J. Gómez, A. U. Alvi, W. ul Hassan, M. Willander and R. Notzel, InN/InGaN quantum dot photoelectrode: efficient hydrogen generation by water splitting at zero voltage. *Nano Energy* 2015, **13**, 291-297.
5. M. Zhong, T. Hisatomi, Y. Sasaki, S. Suzuki, K. Teshima, M. Nakabayashi, N. Shibata, H. Nishiyama, M. Katayama, T. Yamada and K. Domen, Highly active GaN-stabilized Ta_3N_5 thin-film photoanode for solar water oxidation. *Angew. Chem. Int. Ed.* 2017, **56**, 4739-4743.
6. Z. Xu, S. Zhang, F. Gao, P. Gao, Y. Yu, J. Lin, J. Liang and G. Li, Enhanced charge separation and interfacial charge transfer of InGaN nanorods/C_3N_4 heterojunction photoanode. *Electrochim. Acta* 2019, **324**, 134844.
7. J. Miao, H. B. Yang, S. Y. Khoo and B. Liu, Electrochemical fabrication of ZnO-CdSe core-shell nanorod arrays for efficient photoelectrochemical water splitting. *Nanoscale* 2013, **5**, 11118-11124.
8. H. He, S. P. Berglund, P.; Xiao, W. D. Chemelewski, Y. Zhang and C. B. Mullins, Nanostructured Bi_2S_3/WO_3 heterojunction films exhibiting enhanced photoelectrochemical performance. *J. Mater. Chem. A* 2013, **1**, 12826-12834.
9. X. Wang, J. Xie and C. M. Li, Architecting smart "umbrella" Bi_2S_3/rGO-modified TiO_2 nanorod array structures at the nanoscale for efficient photoelectrocatalysis under visible light. *J. Mater. Chem. A* 2015, **3**, 1235-1242.
10. J. Zhang, L. Wang, X. Liu, X. Li and W. Huang, High-performance CdS-ZnS core-shell nanorod array photoelectrode for photoelectrochemical hydrogen generation. *J. Mater. Chem. A* 2015, **3**, 535-541.
11. Y. Zhong, Z. Li, X. Zhao, T. Fang, H. Huang, Q. Qian, X. Chang, P. Wang, S. Yan, Z. Yu, Z. Zou, Enhanced water-splitting performance of perovskite $SrTaO_2N$ photoanode film through ameliorating interparticle charge transport. *Adv. Funct. Mater.* 2016, **26**, 7156-7163.
12. K. Ueda, T. Minegishi, J. Clune, M. Nakabayashi, T. Hisatomi, H. Nishiyama, M. Katayama, N. Shibata, J. Kubota, T. Yamada and K. Domen, Photoelectrochemical oxidation of water using $BaTaO_2N$ photoanodes prepared by particle transfer method. *J. Am. Chem. Soc.* 2015, **137**, 2227-2230.
13. W. Yang, J. H. Kim, O. S. Hutter, L. J. Phillips, J. Tan, J. Park, H. Lee, J. D. Major, J. S. Lee and J. Moon, Benchmark performance of low-cost Sb_2Se_3 photocathodes for unassisted solar overall water splitting. *Nat. Commun.* 2020, **11**, 861.
14. L. Meng, M. Wang, H. Sun, W. Tian, C. Xiao, S. Wu, F. Cao and L. Li, Designing a transparent $CdIn_2S_4/In_2S_3$ bulk-heterojunction photoanode integrated with a perovskite solar cell for unbiased water splitting. *Adv. Mater.* 2020, **32**, 2002893.
15. S. Zhang, L.; Shen, T. Ye, K. Kong, H. Ye, H. Ding, Y. Hu and J. Hua, Noble-metal-free perovskite-$BiVO_4$ tandem device with simple preparation method for unassisted solar water splitting. *Energy Fuels* 2020, **34**, 5016-5023.
16. D. K. Lee and K. S. Choi, Enhancing long-term photostability of $BiVO_4$ photoanodes for solar water splitting by tuning electrolyte composition. *Nat. Energy* 2018, **3**, 53-60.
17. D. Huang, K. Wang, L. Yu, T. H. Nguyen, S. Ikeda and F. Jiang, Over 1% efficient unbiased stable solar water splitting based on a sprayed Cu_2ZnSnS_4 photocathode protected by a HfO_2 photocorrosion-resistant film. *ACS Energy Lett.* 2018, **3**, 1875-1881.
18. H. Son, Y.-J. Choi, J. Hwang and D.-W. Jeon, Influence of post-annealing on properties of alpha-Ga_2O_3 epilayer grown by halide vapor phase epitaxy. *ECS J. Solid State Sci. Technol.* 2019, **8**, Q3024-Q3027.
19. H. Nagakawa and M. Nagata, *In situ* Synthesis of CdS/$CdWO_4$ nanorods core-shell composite *via* acid dissolution. *RSC Adv.* 2020, **10**, 105-111.
20. S. Ye, W. Shi, Y. Liu, D. Li, H. Yin, H. Chi, Y. Luo, N. Ta, F. Fan, X. Wang and C. Li, Unassisted photoelectrochemical cell with multimediator modulation for solar water splitting exceeding 4% solar-to-hydrogen efficiency, *J. Am. Chem. Soc.* 2021, **143**, 12499-12508.